

Comparative Study of Two InGaAs-Based Reference Radiation Thermometers

H. Nasibov¹  · A. Diril¹ · O. Pehlivan¹ · M. Kalemci¹

Received: 23 August 2016 / Accepted: 2 May 2017 / Published online: 18 May 2017
© Springer Science+Business Media New York 2017

Abstract More than one decade ago, an InGaAs detector-based transfer standard infrared radiation thermometer working in the temperature range from 150 °C to 1100 °C was built at TUBITAK UME in the scope of collaboration with IMGC (INRIM since 2006). During this timescale, the radiation thermometer was used for the dissemination of the radiation temperature scale below the silver fixed-point temperature. Recently, a new radiation thermometer with the same design but with different spectral responsivity was constructed and employed in the laboratory. In this work, we present the comparative study of these thermometers. Furthermore, the paper describes the measurement results of the thermometer's main characteristics such as the size-of-source effect, spectral responsivity, gain ratio, and linearity. Besides, both thermometers were calibrated at the freezing temperatures of indium, tin, zinc, aluminum, and copper reference fixed-point blackbodies. The main study is focused on the impact of the spectral responsivity of thermometers on the interpolation parameters of the Sakuma–Hattori equation. Furthermore, the calibration results and the uncertainty sources are discussed in this paper.

Keywords Calibration · Fixed-point blackbody · Pyrometer · Radiation thermometer · Temperature · The Sakuma–Hattori equation

Selected Papers of the 13th International Symposium on Temperature, Humidity, Moisture and Thermal Measurements in Industry and Science.

✉ H. Nasibov
humbet.nasibli@tubitak.gov.tr; humbat.nasibov@gmail.com

¹ TUBITAK UME, Kocaeli, Turkey

1 Introduction

Radiation thermometers due to their noninvasive nature of the temperature measurements and fast responses present a variety of benefits in process controlling for many fields, ranging from fundamental researches to industrial applications. Recently, the demand for the calibration of near-infrared radiation (NIR) thermometers below 1000 °C has increased considerably. Achievements in NIR photodetectors and optical interference filters (with a variety of peak wavelength and bandwidth selection availability) accelerated the developments of pyrometers working in the 150 °C–1100 °C temperature range, often referred as the mid-temperature range. On the other hand, a fixed-point method [1], (where the radiation thermometers are directly calibrated at a number of fixed-point (FP) blackbodies from In FP (156 °C) to the Cu FP (1084 °C)) accompanied with the interpolation equation by Sakuma and Hattori [2] dramatically increased the accuracy of the radiation temperature measured by standard infrared radiation thermometers. Recently, the achievement of 10 mK ($k = 2$) thermodynamic temperature measurement uncertainties at the In-point for a detector-based temperature scale was reported in [3]. As a consequence of this fact, a series of interlaboratory comparisons have been conducted [4–6].

The first transfer standard infrared radiation thermometer (TRT1) was built in 2003 at UME in the scope of collaboration with IMGC. The mechanical, optical, and electrical specifications of both thermometers are similar to the specifications of the transfer standard infrared thermometer developed in INRIM for the temperature range 150 °C to 1000 °C and described in [7]. The main difference between UME and INRIM thermometers is the target-to-objective distance, 590 mm versus 470 mm, respectively.

The second UME InGaAs thermometer (TRT2) was built in 2015 and modified in 2016. The main difference between the two UME radiation thermometers is the spectral responsivity. Both thermometers have a central wavelength around 1600 nm: TRT1 has a top-hat broadband interference filter with a bandwidth (FWHM) of 100 nm, while TRT2 has a Gaussian shape narrow interference filter with the FWHM of 30 nm.

The aim of this work is to compare both UME thermometer's main characteristics and calibration results. Since most of the optomechanical and electrical components of the thermometers are identical, the main characteristics such as size-of-source effect (SSE), gain ratio, and linearity can be tested on the same measurement setup with the same measurement uncertainty. Besides, both thermometers were calibrated against the same FP blackbodies, including freezing temperatures of indium, tin, zinc, aluminum, and copper. Under these conditions, it is expected that the overall comparison of thermometers will be performed with relatively low uncertainty conditions, and consequently, the impact of the variation of the interference filter parameters on the scale approximation equations will be explored more accurately. The paper starts by the comparative study of the main functional characteristics of the thermometers. Thereafter, the calibration results obtained against the FP blackbodies are presented in Sect. 3. Next, the measurement and the Sakuma–Hattori equation interpolation results, uncertainty sources, and the differences between the temperature scales realized through each thermometer are discussed in Sect. 4. Finally, conclusions are summarized in Sect. 5.

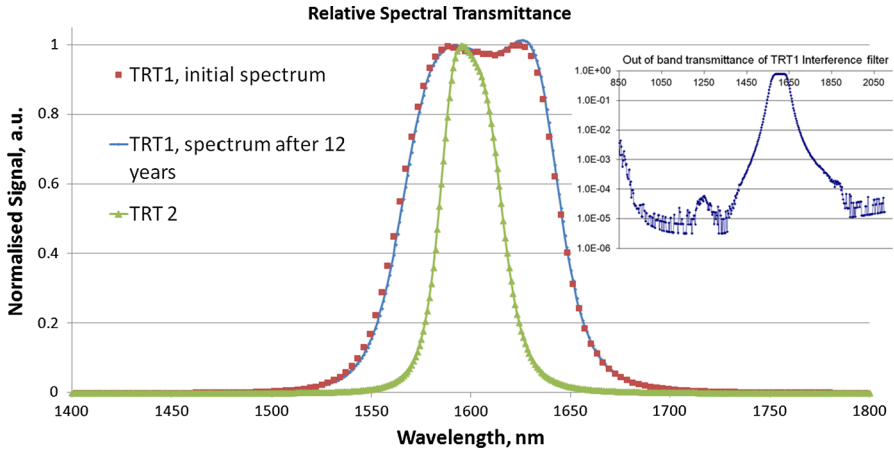


Fig. 1 The relative spectral transmittance of the interference filters, utilized in the TRT1 (dashed-square plot measured in the year 2003, and solid line—measured, in the year 2016) and TRT2 (triangle plot). The inset depicts the out-of-band blocking of the TRT1's interference filter

2 Characterization of the Two InGaAs Radiation Thermometers

2.1 Relative Spectral Transmittances

As mentioned above, two UME thermometers differ from each other by the working spectral bandwidth. TRT1 has a broadband interference filter with a transmittance from about 1500 nm to 1700 nm. Figure 1 shows the relative spectral transmittance of this interference filter that was measured in 2003 by using a single grating monochromator and a lock-in amplifier. The inset in Fig. 1 depicts the out-of-band blocking of the TRT1 interference filter, which is better than 1×10^{-5} . In 2016, the relative spectral transmittance of the TRT1's interference filter was measured again using an Agilent Cary 5000 UV-Vis-NIR spectrometer with a resolution of 1 nm. It was found that, within the resolution of the spectrometer (1 nm), no degradation was observed in the relative spectral transmittance of TRT1's interference filter during the past 12 years. The interference filter TRT2 has a center wavelength of 1600 nm and bandwidth of 30 nm. The relative spectral transmittance of TRT2's interference filter was also measured on the Agilent Cary 5000 UV-Vis-NIR spectrometer. All spectral transmittance results are shown in Fig. 1.

2.2 Size-of-Source Effect (SSE)

The SSE measurements of both thermometers were performed on the same setup by employing the indirect method [8,9]. An integrating sphere (with a diameter of 400 mm) comprising one output port with a diameter of 60 mm was used in measurements. The sphere comprises four incandescent lamps (connected in series) inside. Besides, for minimizing the specular reflection at the output port of the sphere, four internal baffles are placed at specific locations inside the sphere. The lamps are supplied

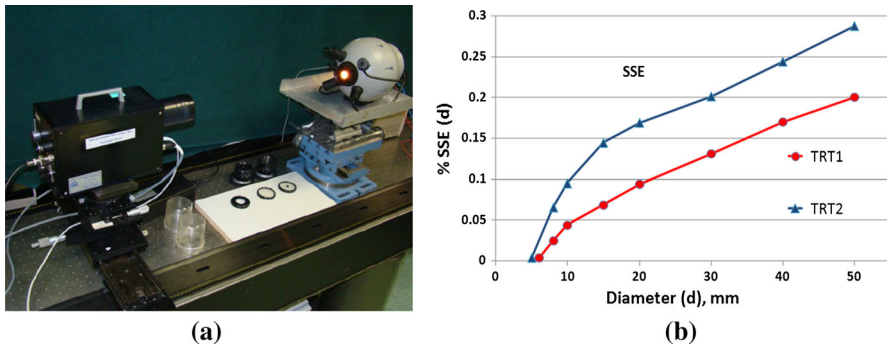


Fig. 2 (a) The SSE measurement setup; (b) The SSE measurement results (circles—TRT1 and triangles—TRT2)

by a controlled DC current, and are switched on at least one hour before the measurements for establishing the quasi-isothermal condition. Apertures with a diameter of 6 mm, 8 mm, 10 mm, 15 mm, 20 mm, 30 mm, 40 mm and 50 mm were used to imitate a variable-diameter source. A black spot of 6 mm in diameter was used as a target. The black spot is fixed in the middle of a glass window. In order to exclude the influence of this supporting glass window's transmittance in the SSE measurements, another identical glass window without the spot (a blank glass window) was used in combination with the apertures. The measurements were performed at 590 mm from the outer surface of the black spot. The transmittance of the spot at the working wavelength band of the thermometers was assessed to be smaller than 0.01%. Figure 2a shows the TRT1 and the SSE measurement setup. The SSE was calculated using the following equation:

$$SSE = (S_{spot} - S_{dark}) / (S_{aperture} - S_{dark}). \quad (1)$$

Here S_{dark} is the relevant dark signal, S_{spot} is the signal measured when the thermometer is focused on the black spot, and $S_{aperture}$ is the signal measured when the aperture is combined with the blank glass window. This measurement is repeated with all apertures of varying internal diameters. The results are shown in Fig. 2b. As it can be seen from Fig. 2b, TRT2 has a larger SSE compared to TRT1. We believe that this deviation originates from the TRT2's achromat doublet entrance lens. Although both achromat doublets were obtained from the same manufacturer (but at different times) and have identical optical specifications (including scratch-dig values), during the optical alignment process we observed that the TRT2's objective lens demonstrates more light scattering (on the field stop) than TRT1's objective lens. One may assume that the relatively large scattering in the TRT2's achromat doublet originates from the imperfections of the cement which is used for gluing the elements of the doublet.

2.3 Nonlinearity Measurements

The detectors in both pyrometers are the same type, glass windowed with an active area of 5 mm in diameter, manufactured by Hamamatsu (G5832-15). The detectors

are thermoelectrically cooled down to $-10\text{ }^{\circ}\text{C}$. As mentioned above, controlling electronic circuits and the transimpedance amplifiers of the thermometers were constructed using the same design, but in different years. In this work, we performed nonlinearity measurements of the detectors and transimpedance amplifiers separately, as described in next section.

2.3.1 The Nonlinearity Measurements of an InGaAs Photodetectors

A variety of methods have been proposed for the nonlinearity measurements of detectors. However, two methods namely “superposition method” and “dual-aperture method” are most widely used in radiometry and pyrometry. An accurate comparison of these methods in the scope of the pyrometry was performed in [10]. Most recently, a novel nonlinearity measurement method of optical detectors that uses light-emitting diodes (LED) has been proposed in [11]. Although this method is also based on the “superposition method” and uses a flux addition technique of radiances of two high brightness LEDs switched by a certain way, the data acquisition and signal processing algorithm is entirely different from conventional lamp-based nonlinearity measurement methods. Besides, the method is very simple and fast, and as shown in [12], an accuracy of 10^{-5} can be reached.

In the current work, the nonlinearities of both thermometers were examined by means of LED-based linearity tester. Since the pyrometers have the same type of InGaAs detectors, the nonlinearity measurements of the detectors were performed on the same experimental setup. In experiments, an NIR LED (Thorlabs, LED1550L) with 120 nm bandwidth and peak wavelength at about 1550 nm were used.

Two arrays of LEDs (each comprising 9 units connected in series) were used in the experiments. By this way, it was possible to reach the sufficient radiant flux at one third of the nominal forward current. The LED arrays are operated at room temperature without temperature stabilization. Additionally, we checked the shift of the peak emission wavelength [13] using the NIR spectrometer, and found that the shift is less than 2 nm. The LED arrays are mounted on ports of an integrating sphere with a diameter of 100 mm. The integrating sphere has three ports, where the centers of two ports (where the arrays are installed) are laying on the same axis, while the third port is perpendicular to this axis (where a detector was installed). The two arrays are driven by two independent current sources (Keithley, model 2400). The photocurrent from the detector is measured using a calibrated pico-ammeter (Keithley, model 196). The arrays are forwarded from $1\text{ }\mu\text{A}$ to 30 mA with certain steps. Before measurements, both arrays were monitored at the conditions described in [14], and an optimal data acquisition at quasi-linear drift mode was established. At each forward current value, 15 data were recorded, and the last 7 data were averaged and were used in further calculations. The nonlinearity correction factor was calculated using the algorithm described in [11]. All of the instruments and measurement routines were controlled by in-house written software.

First, the nonlinearity measurements of the detectors were performed in the overfilled illumination condition [15]. Figure 3a and b shows the results of these nonlinearity measurements, where the plots with the solid circles represent the mean nonlinearity ratios (each measured five times during 3 days) against the mean photocur-

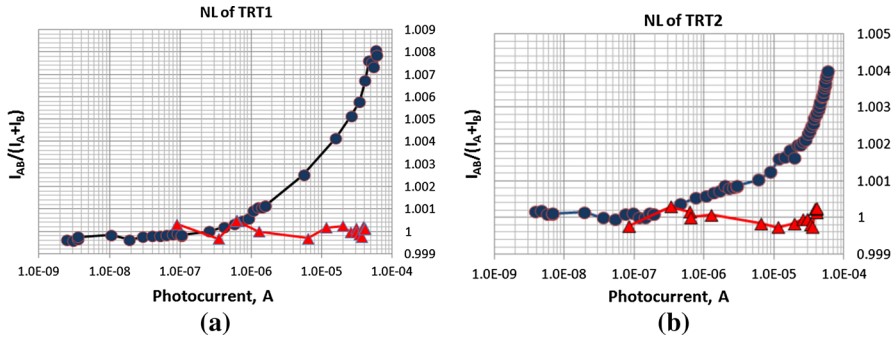


Fig. 3 The measured nonlinearities of (a) TRT1, and (b) TRT2 detectors. The plots with the solid circles correspond to the overfilled illumination condition, while the solid triangles are the results of the underfilled illumination condition (at the aperture diameter of 1.9 mm)

rent values. The results are in good agreement with the data from literature [10, 12]. As it can be seen from Fig. 3, the TRT2's detector has relatively less nonlinear behavior than the TRT1's detector.

Next, the nonlinearity of the detectors were examined in an underfilled illumination condition [15, 16]. In these experiments, a circular aperture stop made from anodized aluminum with an active aperture diameter of 1.9 mm was placed and centered in front of the detector under test.

In order to reach the sufficient radiant flux, we increased the number of LEDs (up to 20 LEDs) in each array by adding extra NIR LEDs: six of aforementioned LEDs were Thorlabs LED1550 and five of them was Thorlabs LED1600L. The injection current supplied to each LED array varied from 0.1 mA to 100 mA. At 100 mA injection current, a maximum output signal of detectors was about of 42 μA . This value is higher than the Cu FP signal of TRT2 (about 13 μA) and slightly lower (about 55 μA) than the corresponding signal of TRT1. The nonlinearity measurements at underfilled illumination condition with the aperture were noted over about three decades (from 8.8×10^{-8} A to 4.2×10^{-5} A). The average of two measurement results is shown in Fig. 3a and b with the solid triangles. As it can be seen from these plots, in the underfilled illumination condition, both InGaAs detectors can be regarded as linear [15–17]. According to these results, no nonlinear corrections were applied to the FP calibration outputs of the thermometers.

2.3.2 Preamplifier Gain Nonlinearity and Ratios

Another source of the nonlinearity of a pyrometer's output signal is the transimpedance amplifier. In pyrometers, this amplifier is employed to extract a photocurrent from the detector and to convert it to an amplified voltage without significantly degrading the intrinsic signal-to-noise ratio. Both thermometers have an amplifier with six gain settings, ranging from $\times 10^5 \text{ V} \cdot \text{A}^{-1}$ to $\times 10^{10} \text{ V} \cdot \text{A}^{-1}$. The detailed description of the employed transimpedance amplifiers, as well as their calibration method is described in [18]. Briefly, the measurements of the amplifier's gain factors were performed by means of a setup shown in Fig. 4a. Here, in order to generate a current of a desired

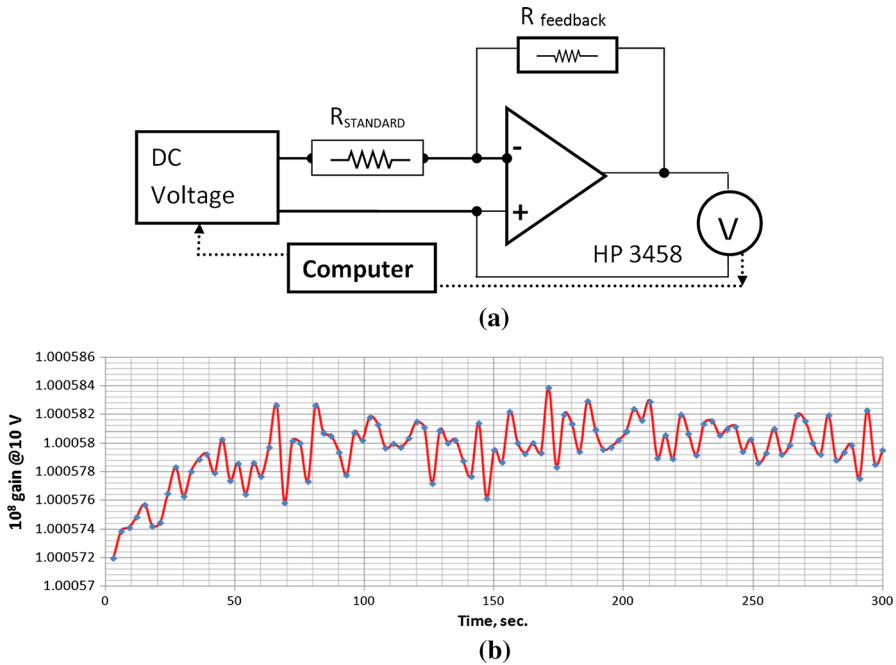


Fig. 4 (a) Schematic diagram of the amplifiers gain factor measurement setup, (b) An example of the short time stability of gain factor measurements

value, a calibrated standard resistor is connected in series to the output of a computer-controlled and calibrated DC voltage source. This current is supplied to the input of the amplifier under test. For each gain setting, a standard resistor with a nominal value that matches with the value of the corresponding feedback resistor of the amplifiers was used. At each gain setting, the gain factor G ($V \cdot A^{-1}$) is calculated from the equation:

$$G = V_{amp} / \left(\frac{V_{cal}}{R_{St}} \right), \tag{2}$$

where V_{amp} is the amplifier output voltage, R_{St} is the value of the standard resistor, and V_{cal} is the output voltage of the DC voltage source. During measurements, V_{cal} is varied from 0.1 V to 1 V with a step of 0.1 V and from 1 V to 10 V with a step of 1 V. In-house written software is used to adjust the output voltage of the calibrator to a desired value and to acquire the signals from a digital multimeter (HP-3458a) that is used to measure V_{amp} .

Figure 4b illustrates an example of the stability of the 10^8 gain versus time during 5 min. The obtained gain ratio values of TRT1 (second column) and TRT2 (fourth column) are shown in Table 1. It is worth to note here that these gain ratio values are in a good agreement with those obtained at the corresponding to the FP signals during the freezing plateau (Table 1, third column for TRT1 and fifth column for TRT2).

Table 1 The gain ratios of the thermometers

Gain ratios	TRT1		TRT2	
	Electrically measured	Calculated from FP signals	Electrically measured	Calculated from FP signals
G10/G9	9.1834	9.186 (± 0.003)	9.212	9.210 (± 0.004)
G9/G8	10.9804	10.982 (± 0.002)	10.9757	10.972 (± 0.003)
G8/G7	10.0623	10.059 (± 0.002)	10.0348	10.035 (± 0.002)
G7/G6	9.8784	9.880 (± 0.002)	9.9442	9.944 (± 0.002)
G6/G5	10.0533	10.054 (± 0.002)	9.9960	9.999 (± 0.002)

As it can be seen from Table 1 the gain ratios are deviated from a factor of 10. In the preamplifiers the metal-film-on-ceramic resistors are used to have a low-temperature variation of resistance. These resistors were obtained from three different manufacturers, which caused the deviation of the obtained gain ratios from an expected value of 10. Besides, even for the resistors from the same manufacturer (in the case of the gain factors of $10^5 \text{ V} \cdot \text{A}^{-1}$ and $10^6 \text{ V} \cdot \text{A}^{-1}$ for TRT1), the measured resistance value of the resistors deviated from the assigned values, that resulted in the difference of the gain ratio factor from 10.

3 Calibrations Against Fixed-Point Blackbodies

Both thermometers were calibrated at five FP blackbodies (In, Sn, Zn, Al, and Cu). In, Sn, and Zn FP sources were realized in a small transportable furnace [19]. The calibrations at Al and Cu points were realized in a three zone tube furnace. Figure 5 illustrates the normalized to the maximum value temperature profile scans across the radiating surface of the FP blackbodies at Zn and Cu points. The scans were performed in the horizontal direction with the TRT1 in the range of $\pm 13 \text{ cm}$, and with the TRT2 in the range of $\pm 8.5 \text{ cm}$ from the center of the cavities.

The FP blackbodies and crucibles were made from high-purity graphite with less than 10 ppm ash content. The blackbodies have a cylindrical cavity with an aperture of 9 mm in diameter and 61.5 mm in height. The back wall of the cavities has a cone shape with 120° included angle. The emissivity of the cavities was estimated as about 0.99957 by assuming a value of 0.9 for the emissivity of graphite and isothermality during phase transitions. The detailed description of the blackbodies used in this study is found in [20].

As it was described in previous section, the wavelength bandwidth of the TRT2 is narrower than the TRT1. Consequently, the output signal of the TRT2 obtained at the same temperature is lower than the signal of TRT1. Figure 6 illustrates the examples of the In FP freezing plateaus obtained by the thermometers at the same gain value. Table 2 depicts the resolution of the thermometers in terms of noise equivalent temperature calculated from the freezing plateaus of the In, Sn, and Zn fixed-points.

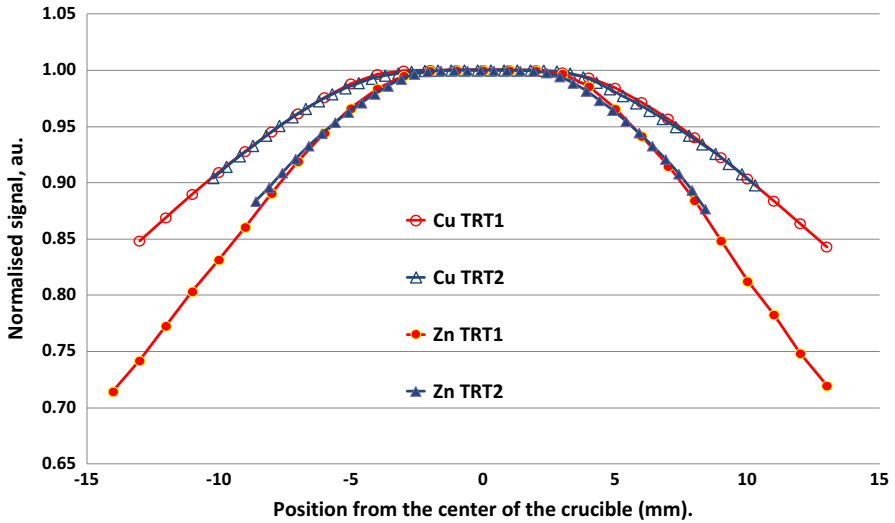


Fig. 5 The normalized temperature profiles (in the horizontal direction) across the Zn point crucible in the small furnace (solid markers) and the Cu point crucible (open markers) in the three zone furnace, obtained by TRT1 (circles) and TRT2 (triangles)

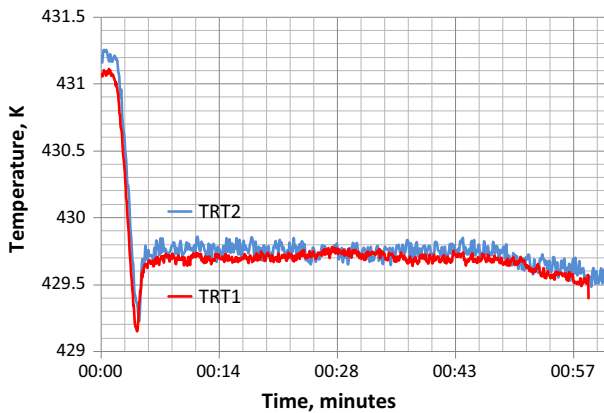


Fig. 6 Typical In FP freezing plateaus obtained by TRT1 and TRT2

Table 2 The comparison results in terms of noise equivalent temperature of thermometers NET (mK)

	In (mK)	Sn (mK)	Zn (mK)
TRT1	18.4	0.76	0.066
TRT2	45.5	0.89	0.17

4 Results and Discussion

The FP calibration outputs of the thermometers were normalized to one gain setting. Table 3 depicts the obtained data for both thermometers.

Table 3 The calibrations results

FP	ITS-90 freezing temperature, (K)	TRT1 normalized output signal ($\times 10^{-6}$ A)	TRT2 normalized output signal ($\times 10^{-6}$ A)
In	429.7485	3.52435×10^{-5}	7.93979×10^{-6}
Sn	505.078	7.86759×10^{-4}	1.80033×10^{-4}
Zn	692.677	9.58287×10^{-2}	2.23587×10^{-2}
Al	933.473	2.70473×10^0	6.40418×10^{-1}
Cu	1357.77	5.46132×10^1	1.31082×10^1

Table 4 The interpolation coefficients

Coefficients	TRT1	TRT2
A (m)	1.599070×10^{-6}	1.591380×10^{-6}
B (m \times K)	2.018630×10^{-6}	2.280570×10^{-6}
C (A)	4.098501×10^4	1.014869×10^4

These results are fitted using the well-known and commonly used interpolation equation—the Sakuma–Hattori equation [21, 22]:

$$S = C \cdot \exp\left(\frac{-c_2}{AT + B}\right), \quad (3)$$

where S is the normalized output signal, T -is the target temperature, $c_2 = 0.014388$ m \cdot K, and A , B , and C are the characteristic constants determined by the spectral characteristics of each radiation thermometer [22]. The obtained interpolation coefficients (A , B , and C) for both thermometers are given in Table 4.

As it can be seen from Table 4, the values of coefficients, denoted by “ A ” in Sakuma–Hattori equation, are very close for both thermometers. According to [22], the coefficient “ A ” is generally understood that is close to the center wavelength of the pyrometer spectral responsivity, which is roughly equal to 1600 nm for both thermometers. The coefficient denoted by “ B ” is treated as the temperature dependence of the effective wavelength. Finally, coefficient denoted by “ C ” is related to the area under the absolute spectral responsivity curve, which is larger for TRT1 than for TRT2, as it is expected. Table 5 depicts the results of the curve fitting using Eq. 3 and coefficients from Table 4.

The comparison of uncertainties in the fixed-point measurements is summarized in Table 6. The uncertainty budget for the comparison is based on the uncertainty sources identified in [23]. However, the uncertainty components from the radiation source, i.e., emissivity, impurity of metals, and furnace temperature gradients, were not considered in the uncertainty budget for the comparison of the thermometers at the fixed points since same fixed-point cells inside same furnaces were used for both thermometers which should cancel these contributions for a comparison.

Table 5 The interpolation results

FP	ITS-90 freezing temperatures, (K)	TRT1			TRT2		
		Interpolated signal, ($\times 10^{-6}$ A)	Residuals ($\times 10^{-6}$ A)	ΔT , (K)	Interpolated signal, ($\times 10^{-6}$ A)	Residuals ($\times 10^{-6}$ A)	ΔT , (K)
In	429.7485	$3.51\ 842 \times 10^{-5}$	$-5.93\ 934 \times 10^{-8}$	-0.0348	$7.94\ 196 \times 10^{-6}$	$2.16\ 512 \times 10^{-9}$	0.0056
Sn	505.078	$7.85\ 524 \times 10^{-4}$	$-1.23\ 562 \times 10^{-6}$	-0.0448	$1.79\ 583 \times 10^{-4}$	$-4.50\ 174 \times 10^{-7}$	-0.0711
Zn	692.677	$9.58\ 281 \times 10^{-2}$	$-6.88\ 870 \times 10^{-7}$	-0.0004	$2.23\ 593 \times 10^{-2}$	$5.82\ 136 \times 10^{-7}$	0.0014
Al	933.473	$2.70\ 472 \times 10^0$	$-1.53\ 612 \times 10^{-5}$	-0.0006	$6.40\ 431 \times 10^{-1}$	$1.20\ 462 \times 10^{-5}$	0.0018
Cu	1357.77	$5.46\ 131 \times 10^1$	$-2.13\ 534 \times 10^{-4}$	-0.0008	$1.31\ 084 \times 10^1$	$1.69\ 620 \times 10^{-4}$	0.0026

Table 6 Uncertainty of comparison of FP measurements for TRT1 (denoted as T1) and TRT2 (denoted as T2)

Uncertainty component	In (mK)		Sn (mK)		Zn (mK)		Al (mK)		Cu (mK)	
	T1	T2	T1	T2	T1	T2	T1	T2	T1	T2
Impurity effect	0	0	0	0	0	0	0	0	0	0
Furnace temperature gradients	0	0	0	0	0	0	0	0	0	0
Plateau determination	20	52	2	2	2	1	16	28	21	38
Emissivity	0	0	0	0	0	0	0	0	0	0
Size-of-source effect	2	2	3	3	5	5	10	10	20	20
Ambient conditions	0	0	1	1	1	1	2	2	4	4
Amplifier gain	4	4	5	5	0	10	10	10	8	8
Multimeters	1	3	0	0	0	0	0	0	0	2
Repeatability of plateaus	29	77	4	16	15	15	30	77	26	74
Reproducibility of plateaus	46	129	8	13	19	22	39	122	37	126
Standard uncertainty	58	159	19	21	27	29	54	148	55	152
Expanded uncertainty ($k=2$)	116	318	39	43	53	58	107	295	110	304

Both thermometers have a calibrated platinum resistance thermometer located in its interior near the filter-detector assembly. The internal temperature of the pyrometers was monitored during the FP realizations. During the calibrations at the Al and Cu points, the internal temperature of the pyrometers increased and this affected the repeatability and reproducibility of the plateaus.

The results of these investigations showed that the contributions due to low signal level of the TRT2 pyrometer at indium FP temperature and the influence of the internal temperature of the thermometers to their responsivity are the two main contributors into the uncertainty budget. Therefore, in the near future, the influence of ambient temperature and humidity on the thermometer's responsivity will be investigated and the results of the experiments will be published elsewhere.

5 Conclusion

Two transfer standard radiation thermometers having the same optomechanical and electrical specifications, but different spectral responsivities have been compared by the calibration against the FP (In, Sn, Zn, Al and Cu) blackbodies. The first thing to say is that the interpolation coefficients for the Sakuma–Hattori equation obtained from the experimental results in the current work corresponds to the theoretical predictions based on the physical interpretation of the interpolation equation parameters for radiation thermometry [22].

Besides, it was shown that, the low signal level in In FP for the TRT2 thermometer (with a narrow spectral bandwidth) is one of the main sources in the uncertainty budget of the scale approximation in the temperature range from 150 °C to 1100 °C. Therefore, it was decided for the realization of the radiation temperature scale in the

aforementioned temperature range at TUBITAK UME to use the TRT1 thermometer (with a relatively wide spectral bandwidth). In addition, the results of these investigations showed that the influence of the internal temperature and humidity of the thermometers are the second relatively large uncertainty sources (especially at above Zn FP realizations) in the scale approximation. Future work will involve establishing the correction coefficients for the minimizing of the effect of ambient temperature and humidity on the thermometer's responsivity.

Finally, it is worth to note here that the results of preliminary intercomparison between the scales in the temperature range from 600 °C to 1100 °C obtained by the TRT1 thermometer in this work and the current ITS-90 radiation temperature scale of UME (established at 900 nm effective wavelength) are in agreement within 150 mK, and the final results of this intercomparison will be published elsewhere.

Acknowledgements The authors would like to thank the anonymous referees for useful comments and constructive suggestions.

References

1. M. Battuello, F. Lanza, T. Ricolfi, *Metrologia* **27**, 75 (1990)
2. F. Sakuma, S. Hattori, in *Temperature: Its Measurement and Control in Science and Industry*, vol. 5, ed. by J.F. Schooley. AIP Conference Proceedings (New York, 1982). pp. 421–427
3. H.W. Yoon, C.E. Gibson, V. Khromchenko, G.P. Eppeldauer, *Int. J. Thermophys.* **28**, 2076 (2007)
4. X.P. Hao, H.C. McEvoy, G. Machin, Z.D. Yuan, T.J. Wang, *Meas. Sci. Technol.* **24**, 075004 (2013)
5. F. Girard, T. Ricolfi, in *Proceedings of TEMPMEKO 2004, 9th International Symposium on Temperature and Thermal Measurements in Industry and Science* (Dubrovnik, Croatia, 2004), pp. 827–732
6. M. Battuello, F. Girard, T. Ricolfi, in *Temperature: Its Measurement and Control in Science and Industry*, vol. 7, ed. by D.C. Ripple. AIP Conference Proceedings (Chicago, 2002). pp. 903–908
7. T. Ricolfi, F. Girard, in *Proceedings of TEMPMEKO 1999, 7th International Symposium on Temperature and Thermal Measurements in Industry and Science* (Delft, 1999), pp. 593–598
8. G. Machin, R.Sergienko, in *Proceedings of TEMPMEKO 2001, 8th International Symposium on Temperature and Thermal Measurements in Industry and Science* (VDE Verlag, Berlin, 2002), pp. 155–160
9. F. Sakuma, L. Ma, Z. Yuan, in *Proceedings of TEMPMEKO 2001, 8th International Symposium on Temperature and Thermal Measurements in Industry and Science* (VDE Verlag, Berlin, 2002), pp. 161–166
10. M. Battuello, P. Bloembergen, F. Girard, T. Ricolfi, *AIP Conf. Proc.* **684**, 613 (2003)
11. D.J. Shin, D.H. Lee, C.W. Park, S.N. Park, *Metrologia* **42**, 154 (2005)
12. D.J. Shin, S. Park, K.L. Jeong, S.N. Park, D.H. Lee, *Metrologia* **51**, 25 (2014)
13. H. Nasibov, E. Balaban, A. Kholmatov, A. Nasibov, *Flow Meas. Instrum.* **37**, 12 (2014)
14. W. Dong, Z. Yuan, P. Bloembergen, X. Lu, Y. Duan, *Int. J. Thermophys.* **32**, 2587 (2011)
15. P. Corredera, M.L. Hernanz, M. Gonzales-Herraez, J. Campos, *Metrologia* **40**, S150 (2003)
16. D.J. Shin, D.H. Lee, G.R. Jeong, Y.J. Cho, S.N. Park, I.W. Lee, in *Proceedings of NEWRAD 2005, 9th International Conference on New Developments and Applications in Optical Radiometry* (Davos, 2005), pp. 77–78
17. H.W. Yoon, J.J. Butler, T.C. Larason, G.P. Eppeldauer, *Metrologia* **40**, S154 (2003)
18. H. Nasibov, S.Ugur, in *Proceedings of IMEKO 2003, 17th World Congress Metrology in the 3rd Millennium* (Dubrovnik, Croatia, 2003), pp. 1702–1705
19. F. Girard, T. Ricolfi, *Meas. Sci. Technol.* **9**, 1215–1218 (1998)
20. A. Diril, H. Nasibov, S. Ugur, in *Temperature: Its Measurement and Control in Science and Industry*, vol. 7, ed. by D.C. Ripple. AIP Conference Proceedings (Chicago, 2002)
21. P. Saunders, D.R. White, *Metrologia* **41**, 41 (2004)
22. P. Saunders, D.R. White, *Metrologia* **40**, 195 (2003)
23. P. Saunders et al., *Int. J. Thermophys.* **29**, 1066 (2008)